Industrial Crops & Products 225 (2025) 120454

Contents lists available at ScienceDirect

Industrial Crops & Products

journal homepage: www.elsevier.com/locate/indcrop

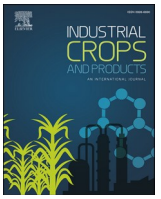

Amazonian Surucucumirá fibers: From native tree to a possible sustainable nano-reinforcement.

Samir Leite Mathias [a], Vitor Hugo de Lima [a], Isabella Karoline Ribeiro Dias [b], Valdeir Arantes [b], Marcelo De Assumpção Pereira-Da-Silva [c,d], Alessandra De Almeida Lucas [e], Aparecido Junior De Menezes [a,*]

[a] Universidade Federal de São Carlos – UFSCar, Sorocaba, SP, Brazil
[b] Escola de Engenharia de Lorena – EEL-USP, Lorena, SP, Brazil
[c] Instituto de Física de São Carlos –IFSC-USP, São Carlos, SP, Brazil
[d] Centro Universitário Central Paulista – UNICEP, São Carlos, SP, Brazil
[e] Universidade Federal de São Carlos – UFSCar, São Carlos, SP, Brazil

ARTICLE INFO

Keywords:
Amazon lignocellulosic fibers
Fast growing tree
Nanocellulose
Renewable sources

ABSTRACT

Cellulose nanocrystals (CNCs) and nanofibrils (CNFs) were obtained from fibers of a native Amazon tree known as Surucucumirá (*Spathelia excelsa* (Krause) Cowan & Brizicky [sin. *Sohnroyia excelsa* K.]). The chemical composition of the biomass was inspected through TAPPI standards and the lignin and alphacellulose contents were, respectively, around 38.9 % and 31.3 %. Fourier Transform Infrared Spectroscopy (FTIR) analysis confirmed the successful removal of lignin and hemicellulose from the raw fibers without disrupting the cellulose's glycosidic bonds. This is further supported by the scanning electron microscopy (SEM) micrographs, which reveal the fibrillation following the bleaching process. Thermogravimetry (TG) results showed the dependence of intermolecular and intramolecular interactions influencing on thermal stability, with CNFs exhibiting higher stability compared to CNCs. X-ray diffraction (XRD) analysis revealed a significant increase in crystallinity, with the Crystallinity Index (CI) rising from 54.1 % for the raw samples to 89.6 % for the nanocellulose samples. Atomic force microscopy (AFM) nanographs confirmed the successful extraction of both CNCs and CNFs.

1. Introduction

The Amazon Phoenix Project, established by Brazil's National Institute for Amazonian Research (INPA) (Nobre, 2012), aims to promote a sustainable and symbiotic relationship between human development and the remaining natural ecosystems of the Amazon. This initiative strives to create a network that fosters economic growth while prioritizing ecological harmony. By encouraging the use of renewable resources, the project seeks to ensure a future where human and environmental well-being are inextricably linked.

The constant search for accessible and useful materials from renewable sources brings us to the discovery of plants and trees that must be planted and harvested on a large scale, always causing problems to the soil. Plants like Surucucumirá (*Spathelia excelsa* (Krause) Cowan & Brizicky [sin. *Sohnroyia excelsa* K.]), a hapaxanthic tree (that blooms and dies), can be planted among other Amazon native trees, like Cupiúba (*Goupia glabra* Aubl.), Cumaru (*Dipteryx odorata* Aubl.), Andiroba (*Carapa guianensis* Aubl.), Castanheira-do-Brasil (*Bertholletia excelsa* Bonpl.), Tatajuba (*Bagassa guianensis* Aubl.) and Mogno-brasileiro (*Swietenia macrophylla* King.) providing shades and protection to these slow-growing species because of his fast-growing, 10–20 m of height and 20 centimeters of diameter in 2 years (Rodrigues, 1962). Besides, the Surucucumirá tree presents very interesting properties that is to neutralize larvae and mosquitos of *Aedes aegypti* and protozoa of *Leishmania braziliensis* and *Trypanossoma cruzi as* the works of Freitas et al. (2009) and Moreira et al. (2009).

Lignocellulosic fibers have a wide range of application due to their unique properties and potential for sustainable material production. The use of lignocellulosic nanomaterials like CNCs and CNFs in polymeric matrices is a large field of research with promising results. These nano-reinforced composites, called nanocomposites, offer several advantages over traditional polymer matrices. Studies have shown improvements in

* Corresponding author.
E-mail address: jrmenezes@ufscar.br (A.J. De Menezes).

https://doi.org/10.1016/j.indcrop.2024.120454
Received 16 July 2024; Received in revised form 11 December 2024; Accepted 31 December 2024
Available online 10 January 2025

mechanical and thermal properties, enhanced barrier properties against both water vapor and gas, and increased biodegradability (Azizi Samir et al., 2005; Bras et al., 2010; Rao et al., 2024; Sanjeevi et al., 2024; Xie et al., 2018).

This study aimed to be the first comprehensive investigation of Surucucumirá fibers. We analyzed the chemical composition of the fibers (cellulose, hemicellulose, lignin, and ash), followed by the extraction of nanocrystals and nanofibrils.

2. Methodology

2.1. Materials

Surucucumirá biomass, obtained from the Amazon Phoenix Project, was cut into ~30 mm pieces and oven-dried (Solab SL-100) at 80 °C for 48 h. The dried material was then ground using a vertical rotor cutting mill (Cienlab CE-430) equipped with mobile blades to achieve a particle size of MESH 80 (180 μm). All chemical reagents, including sulfuric acid (98.0 %), sodium hydroxide (97.0 %), acetic acid (99.7 %), and sodium chlorite (80.0 %), were purchased from Merck and used as received.

3. Methods

3.1. Chemical composition

The chemical compositions were determined according to the TAPPI standards: T222 om-02 (insoluble lignin), T13 m-54 (soluble lignin), T211 om-93 (ash), T257 om-85 (holocellulose - chlorite treatment), and T203 cm-99 (alphacellulose - alkaline treatment). Total lignin content was determined by summing the soluble and insoluble lignin fractions (Mathias et al., 2022). All analyses were performed in triplicate, and the results are reported as average values with their corresponding standard deviations.

3.1.1. CNCs extraction

CNCs were isolated from the bleached fibers via an acid hydrolysis process. The process involved treating 1 g of cellulose with 20 mL of 10 M sulfuric acid at 55 °C for 10 minutes. The reaction was stopped by dilution with deionized ice cubes. The resulting suspension was then thoroughly washed with deionized water using centrifugation (4000 rpm, 20 min) repeated three times. Subsequently, the suspension was dialyzed against deionized water using a 12–14 kDa molecular weight cut-off dialysis membrane (Merck) until the pH approached neutrality.

3.1.2. CNFs extraction

The alphacellulose fibers were defibrillated by disc ultra-refining at 1500 rpm. The cellulosic pulp was briefly diluted in distilled water to 2 % (w/w), and 1 L of the aqueous suspension was defibrillated in the disc ultra-refiner SuperMassColloider (Masuko, model MKCA6–2 J). The cellulosic suspension was repeatedly (20x) passed through the SuperMassColloider.

3.1.3. Fourier transform infrared spectroscopy (FTIR)

The samples were mixed with KBr (1 % w/w) and pressed to pellets, the data were recorded on a Shimadzu IRAffinity-1 spectrometer. The measurements were conducted under a nitrogen atmosphere at room temperature. The analysis utilized a wavenumber range of 4000–600 cm^{-1} , a resolution of 2 cm^{-1} , and 64 scans per sample.

3.1.4. Scanning electron microscopy (SEM)

The surface morphology of the samples was analyzed by scanning electron microscopy (SEM) before and after bleaching. Micrographs were obtained using a Hitachi TM3000 Tabletop Microscope operating at an accelerating voltage of 5 kV without sputtering.

3.1.5. Thermogravimetry (TG)

Thermal stability of the fiber samples was evaluated using a TA Instruments TGA-55 analyzer under a nitrogen atmosphere (30 mL.min^{-1} flow rate). Samples were heated from 30 °C to 500 °C at a rate of 10 °C. min^{-1} in aluminum crucibles.

3.1.6. X-ray diffraction (XRD)

The measurements were performed using a Shimadzu DRX-6100. Cu Kα radiation generated at a voltage of 40 kV and current of 30 mA was utilized with a scan speed of 2°. min^{-1} and 2θ from 5° to 35°.

Segal's method was utilized to calculate the Crystallinity Index (CI) for raw and holocellulose samples (Segal et al., 1959) and Revol et al. (1987) method for cellulose samples, which allows the parallel among samples.

$$CI_{Segal} = \frac{I_{(22.5^\circ)} - I_{(18.6^\circ)}}{I_{(22.5^\circ)}} \quad (1)$$

$$CI_{Revol} = \frac{I_{(20.0^\circ)} - I_{(15.0^\circ)}}{I_{(20.0^\circ)}} (2)$$

Where $I_{(22.5^\circ)}$ and $I_{(20.0^\circ)}$ correspond to the crystalline fraction of cellulose and $I_{(18.6^\circ)}$ and $I_{(15.0^\circ)}$ correspond to the amorphous fraction of cellulose, for type I and type II cellulose, respectively.

3.1.7. Atomic force microscopy (AFM)

The nanographs were acquired using a Bruker Dimension ICON in intermittent contact mode (tapping mode). A silicon rectangular cantilever with a spring constant of 40 N.m^{-1}, vibrating at 330 kHz, was employed to probe the nanocellulose surface. Height and phase images were acquired, with the height data subsequently analyzed using the Nanoscope Analysis software. The equation 3 (Dufresne, 2017) was used to calculate the specific surface area of the nanocrystals, for the density (ρ) was used 1.5 g.cm^{-3} and "d" as the diameter of the CNCs.

$$A_{sp} = \frac{4}{\rho.d} \quad (3)$$

4. Results and discussion

4.1. Chemical composition

The alphacellulose content (Table 1) is lower compared with the other hardwoods from the Amazon region, which is due to its rapid growth (Bodirlau et al., 2007) which is even faster than the *Paulownia elongota* that achieves maturity for harvest within three years with 5 m of height and 20 cm of diameter with around 44 % of alphacellulose. As far as our knowledge goes no information about the chemical composition of Surucucumirá was found in the literature, the comparative was carried out with some species of hardwood tree planted in the Amazon Rainforest with a diameter and height as close as the studied tree.

Amapá-Roxo (*Brosimum parinarioides* Ducke), Embaúba-prateada (*Cecropia hololeuca*), Matamatá-vermelho (*Lecythis idatimon*) and Muirapiranga (*Brosimum paraense* Huber).

5. FTIR

Fig. 1 presents the FTIR spectra of Surucucumirá, raw fiber (before any chemical treatment), holocellulose (after the chlorite treatment), alphacellulose (after the alkaline treatment), CNCs (after the acid hydrolysis), and CNFs (after mechanical treatment). The raw sample is a conglomerate of all lignocellulosic bands that can be confirmed by the bands at 1730 cm^{-1} and 1370 cm^{-1}, respectively OH phenolic group bending and C═O stretching. The intensity of this bands showed a reduction after the chlorite treatment due to the partial lignin removal. The asymmetric stretching of CH_2 and CH, both located between 2800 and 2900 cm^{-1}, are related respectively to alphacellulose groups and

Table 1
Percentual values of the biomass content of the sample and comparatives (Pettersen, 1984).

	Holocellulose (%)	Hemicellulose (%)	Alphacellulose (%)	Lignin (%)	Ash (%)
Surucucumirá	61.51 ± 0.17	30.18 ± 0.79	31.32 ± 0.82	38.93 ± 0.97	0.16 ± 0.02
Amapá-Roxo	-	-	51	26	0.2
Embaúba- Prateada	69	20	49	25	0.7
Matamatá-vermelho	-	-	47	30	0.5
Muirapiranga	-	-	41	38	0.2

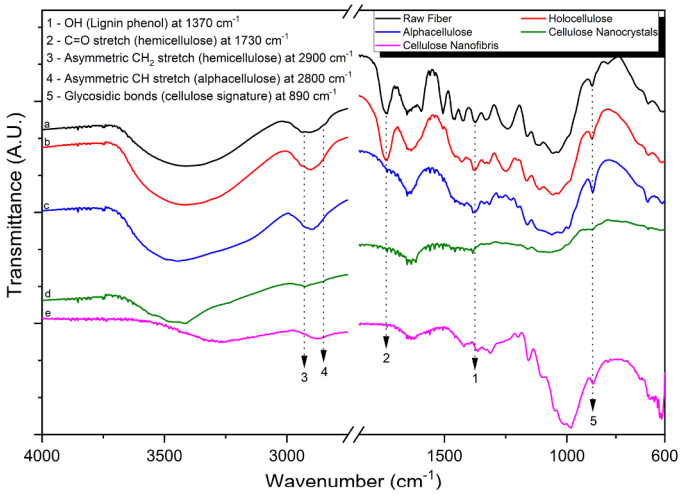

Fig. 1. FTIR spectra from Surucucumirá (*Spathelia excelsa* (Krause) Cowan & Brizicky [sin. *Sohnroyia excelsa* K.]*)* fibers. a, b, c, d and e lines correspond, respectively, to raw, holocellulose, alphacellulose and CNCs samples.

hemicellulose groups, the second one is partially removed after the alkaline treatment. The peak observed at 890 cm^{-1} corresponds to the β-glycosidic bond between anhydroglucose units, a characteristic signature band for cellulose in infrared (IR) spectroscopy (Arun Ramnath et al., 2024; García-Guzmán et al., 2024).

6. SEM

Surucucumirá fibers' structures were scanned through SEM and the results are shown in Fig. 2. It reveals a high linkage between alphacellulose, hemicellulose, and lignin in the raw fibers. Following partial lignin removal via chlorite treatment, the holocellulose column exhibits microcavities indicative of cell wall deconstruction. This alteration enhances the fiber's susceptibility to subsequent chemical attacks. Consequently, the alkaline treatment induces a more extensive breakdown of the fibers (fibrillation) observed in the alphacellulose column (Martins et al., 2021).

7. AFM

The success of the extraction, through sulfuric acid hydrolysis and ultrafine grinder, respectively of Surucucumirá's CNCs and CNFs, can be noted in Fig. 3 where can be seen the CNCs in a rod-like morphology, the most expected morphology by the method used, and CNFs as a thin and long fiber. After the image treatment of CNCs the most well-dispersed nanocrystals (the ones surrounded by dark) were searched and measured length and diameter, only a few were observed due to their high tendency to aggregate which could lead to a wrong measurement where two or more nanocrystals would be overlaid, thus obtaining Table 2, the CNFs were not fully measured because it was not possible to get the length of the fibers, only the diameter.

Some works (Eichhorn et al., 2010; Ghasemi et al., 2023; Sánchez-García et al., 2010) show an insignificant improvement on mechanical properties using low aspect ratio nano-reinforcers, but when it's related to barrier properties the use of short nano-reinforcers shows improvements, creating sinuous path through the matrices that difficult passage of fluids like water or even air. As for the CNFs, with their higher aspect ratio (same diameter but much higher length), an increase in mechanical properties is expected according to the works already mentioned. It's well known (Cadek et al., 2004) that the interactions among matrix and the reinforcers are made by an interfacial phase (or interphase) through van der Waals' forces and hydrogen bonding, this interfacial phase is improved as the specific surface area of the reinforcer increases.

8. TG

Thermogravimetry was employed to evaluate the thermal stability of the raw, holocellulose, alphacellulose, CNCs, and CNFs samples. The observed thermal degradation events across the temperature range are summarized in Table 3 based on the data extracted from Fig. 4.

The thermal degradation profiles for raw fiber, holocellulose, and alphacellulose exhibit three distinct events across the temperature range. The profiles for nanocrystals and nanofibrils display also three events, two of them correspond to the first and third stages observed in the other samples and the third event correspond to char formation.

The first stage (32 ± 5 °C to 111 ± 12 °C) corresponds to the evaporation of water and low molecular weight compounds. The second stage (111 ± 16 °C to 258 ± 24 °C) involves the decomposition of low molecular weight fatty acids and esters. The third stage (occurring at

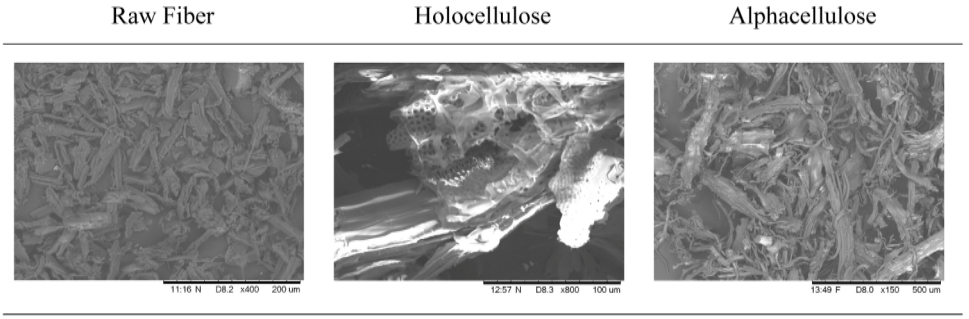

Fig. 2. Scanning electron microscopies of the surucucumirá fibers (100 μm). Raw fiber, holocellulose and alphacellulose as first, second, and third columns.

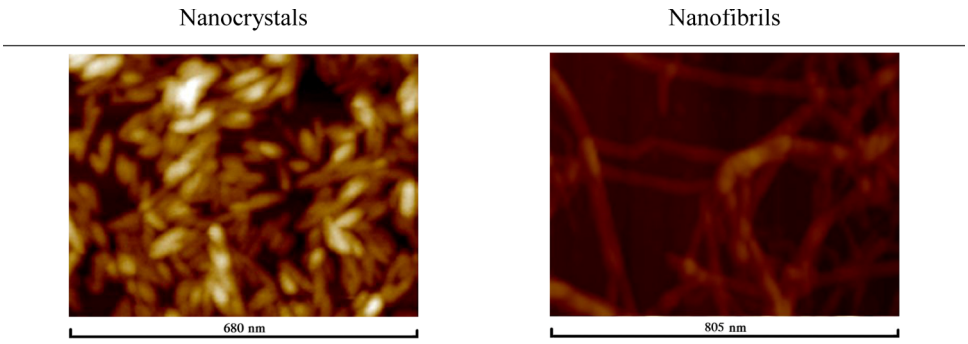

Fig. 3. Atomic Force Microscopy (AFM) of surucucumirá's cellulose nanocrystals and nanofibrils.

Table 2
Length, aspect ratio, specific surface area of the nanocrystals and diameter of nanocrystals and nanofibrils.

	Nanocrystals	Nanofibrils
Length (nm)	80.51 ± 3.55	-
Diameter (nm)	4.94 ± 0.16	4.09 ± 1.34
Aspect ratio	16.30 ± 0.11	-
Specific surface area ($m^2.g^{-1}$)	539.97 ± 139.2	-
Yield (%)	19.68 ± 0.21	48.7 ± 1.3

Table 3
Surucucumirá's thermogravimetry events.

Surucucumirá		*Raw*	*Holo*	*Alpha*	*CNCs*	*CNFs*
Water and low molecular compounds evaporation	T_{onset} (°C)	27.8	27.9	30.6	30.1	45.6
	T_{max} (°C)	43.4	42.2	35.4	42.3	73.9
	ML (%)	3.8	3.0	6.0	0.8	8.1
Decomposition of low molecular weight fatty acids and esters	T_{onset} (°C)	102.1	102.3	130.1	-	-
	T_{max} (°C)	252.2	237.8	283.7	-	-
	ML (%)	4.1	4.6	3.6	-	-
Cellulose degradation	T_{onset} (°C)	252.2	237.8	283.7	147.5	206.0
	T_{max} (°C)	342.9	316.6	336.5	301.3	366.6
	T_{end} (°C)	366.1	382.2	389.9	371.1	416.7
	ML (%)	66.2	64.5	71.7	56.4	59.5

different temperature ranges depending on the sample) is the most complex and involves the decomposition of hemicellulose, pectin, lignin, and glycosidic units, along with dehydration and depolymerization reactions of cellulose. For raw fibers, holocellulose, and alpha-cellulose, this stage occurs between 258 ± 24 °C and 380 ± 12 °C. Interestingly, nanocrystals and nanofibrils exhibit a shift in this stage, with degradation occurring between 147 °C and 371 °C (nanocrystals) and 206 °C and 416 °C (nanofibrils). Above these temperatures for CNFs and CNCs there are only char formation (César et al., 2015; De Morais Teixeira et al., 2010; Garcia Filho et al., 2020; Kalia et al., 2011; Paksung et al., 2020; Sun et al., 2010; Yang et al., 2007).

These three different behaviors that were observed are due to the differences in the inherent structures and the chemical nature of the three main lignocellulosic components (cellulose, hemicellulose and lignin). The various saccharides found in hemicellulose (xylose, galactose, mannose, etc.) are rich in branches and amorphous structures proving a low temperature degradation. Cellulose, as opposed to hemicellulose, consists of long chains of glucose without ramification; it's made of a very ordained and strong structure that ensures a higher thermal stability. That higher temperature range of the raw material it's because of the chemical bonds in the lignin, full of aromatic rings which leads to a high thermal degradation (Yang et al., 2007).

After the acid hydrolysis the sulfate half-ester group (OSO_3^-) is inserted on the outermost hydroxyl (C_6), this insertion causes a catalytic effect in the thermal degradation thus changing the cellulose thermostability, decreasing it (Börjesson et al., 2018; Gan et al., 2020; Imiete et al., 2023; Lin and Dufresne, 2014; Roman and Winter, 2004). CNFs preparation is only forced fibrillation through mechanical forces, because of this there are increases on the T_{onset} and ML (mass loss) of the water evaporation, because the fibrillation leads to a higher specific surface area with more interactions with water molecules, and a slightly reduction on the T_{onset} of the cellulose degradation, the higher the fibrillation the easier the decomposition.

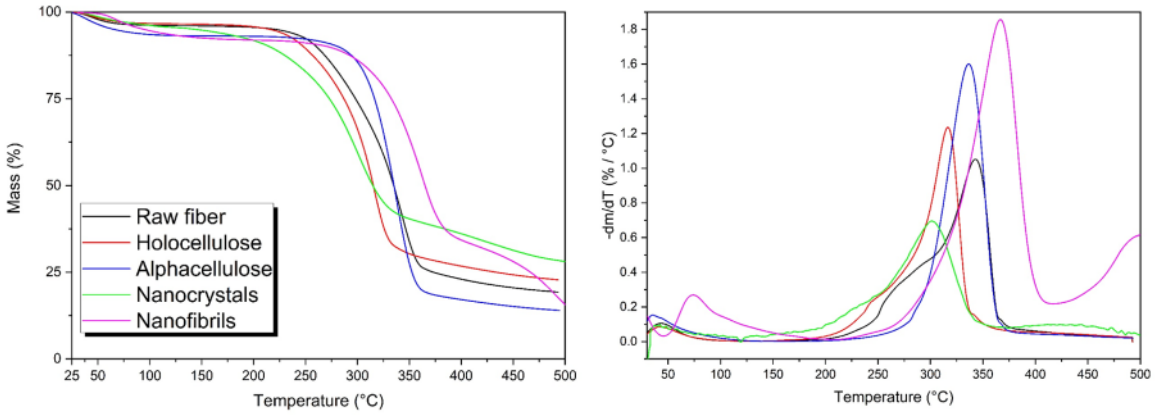

Fig. 4. TG and dTG curves of the raw, holocellulose, cellulose, nanocrystals and nanofibrils of the surucucumirá fibers.

9. XRD

Segal and Revol (French and Santiago Cintrón, 2013; Lee et al., 2017; Nam et al., 2016) works show the description and shapes of lignocellulose diffractograms that can be associated with those shown in Fig. 5, the raw and holocellulose diffractograms exhibit two crystalline peaks a wider one (110) and a sharp one (200) superimpose on an amorphous wide halo, a classical cellulose type I crystallography. The patterns of alphacellulose reveal the emergence of two new crystalline peaks at 12.3° (corresponding to the (1−10)) and 22° (assigned to the (020) reflection). This observation indicates the transformation of cellulose from its original type I structure to type II during the alkaline treatment process (Liu and Hu, 2008; Martins et al., 2015). The Crystallinity Index (CI) from all native species fibers are shown at Table 4.

As expected, the more refined are the fiber higher are the crystallinity index, from raw sample to holocellulose the increase on crystallinity occurs because lignin`s removal, holocellulose to alphacellulose it`s because of the hemicellulose removal, for the nanofibers and nanocrystal the higher crystallinity it`s because of the removal of the amorphous phase by, respectively, mechanical and chemical action.

10. Conclusions

The chemical and physical properties of Surucucumirá (*Spathelia excelsa* (Krause) Cowan & Brizicky [sin. *Sohnroyia excelsa* K.]) were analyzed and showed values consistent with a fast-growing hardwood, the SEM micrographs showed the removal of lignin with the evident microcavities appearing on holocellulose micrograph, and removal of hemicellulose with the evident fibrillation of the cellulose micrograph, the observed decrease in the intensity of lignin-related peaks in the FTIR spectra is corroborated by the micrographs and TG through the temperature range until the pyrolisys.

Acid hydrolysis and mechanical grinding successfully produced suspensions of nanocrystals and nanofibrils, respectively, confirmed by AFM micrograph that showed nanocrystals with rod-like geometry and nanofibrils as a long and thin fiber. The XRD diffractogram showed an expected increase in the crystalline index through the reduction of amorphous phase in the samples. Supported by previous research and the calculated values of the aspect ratio and specific surface area, it was concluded that the CNCs generated through this work present the potential like nano-reinforcements on polymerics matrices and potentially enhance their barrier properties and the CNFs can be used on polymerics matrices to potentially improve the mechanical properties.

CRediT authorship contribution statement

Marcelo de Assumpção Pereira-da-Silva: Writing – review & editing, Writing – original draft, Visualization, Software, Data curation. **Valdeir Arantes:** Writing – review & editing, Methodology, Investigation. **Isabella Karoline Ribeiro Dias:** Methodology, Investigation. **Vitor Hugo de Lima:** Writing – review & editing, Software, Methodology, Investigation. **Samir Leite Mathias:** Writing – review & editing, Writing – original draft, Visualization, Validation, Software, Methodology, Investigation, Formal analysis, Data curation, Conceptualization. **Aparecido Junior de Menezes:** Writing – review & editing, Writing – original draft, Visualization, Validation, Supervision, Software, Resources, Project administration, Methodology, Investigation, Funding acquisition, Formal analysis, Data curation, Conceptualization. **Alessandra de Almeida Lucas:** Writing – review & editing, Supervision, Resources, Methodology, Investigation, Conceptualization.

Declaration of Competing Interest

The authors declare the following financial interests/personal relationships which may be considered as potential competing interests: Samir Leite Mathias reports financial support was provided by Coordination of Higher Education Personnel Improvement. If there are other authors, they declare that they have no known competing financial interests or personal relationships that could have appeared to influence the work reported in this paper

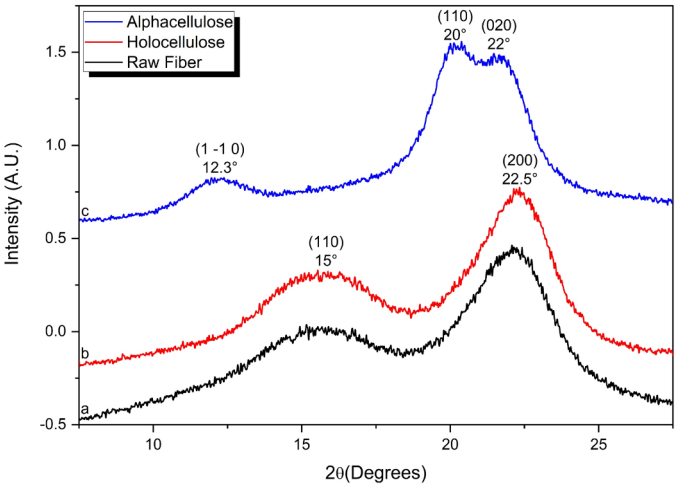

Fig. 5. X-ray Diffractogram of surucucumirá. Raw fiber, holocellulose, alphacellulose are, respectively, a, b, and c lines.

Table 4
Crystallinity Index (CI) of the raw, holocellulose, alphacellulose and nanocrystals sample.

Raw Sample (%)	Holocellulose (%)	Alphacellulose (%)	Nanofibrils (%)	Nanocrystals (%)
54.1	63.9	78.6	81.5	89.6

Acknowledgment

The authors gratefully acknowledge financial support from CAPES, fiber donation from the Amazon Phoenix Project (Projeto Fênix Amazônico), and thermogravimetric analysis measurements provided by PUC-SP.

Appendix A. Supporting information

Supplementary data associated with this article can be found in the online version at doi:10.1016/j.indcrop.2024.120454.

Data availability

Data will be made available on request.

References

Arun Ramnath, R., Senthamaraikannan, P., Gautham, V., Indran, S., Gapsari, F., 2024. Characterization of alkali treated and untreated Abutilon indicum FIBERS. Ind. Crops Prod. 222, 119719. https://doi.org/10.1016/j.indcrop.2024.119719.

Azizi Samir, M.A.S., Alloin, F., Dufresne, A., 2005. Review of recent research into cellulosic whiskers, their properties and their application in nanocomposite field. Biomacromolecules 6, 612–626. https://doi.org/10.1021/bm0493685.

Bodirlau, R., Spiridon, I., Teaca, C.A., 2007. Chemical investigation on wood tree species in a temperate forest, east-northern Romania. BioResources 2, 41–57.

Börjesson, M., Sahlin, K., Bernin, D., Westman, G., 2018. Increased thermal stability of nanocellulose composites by functionalization of the sulfate groups on cellulose nanocrystals with azetidinium ions. J. Appl. Polym. Sci. 135. https://doi.org/10.1002/app.45963.

Bras, J., Hassan, M.L., Bruzesse, C., Hassan, E.A., El-Wakil, N.A., Dufresne, A., 2010. Mechanical, barrier, and biodegradability properties of bagasse cellulose whiskers reinforced natural rubber nanocomposites. Ind. Crops Prod. 32, 627–633. https://doi.org/10.1016/j.indcrop.2010.07.018.

Cadek, M., Coleman, J.N., Ryan, K.P., Nicolosi, V., Bister, G., Fonseca, A., Nagy, J.B., Szostak, K., Béguin, F., Blau, W.J., 2004. Reinforcement of polymers with carbon nanotubes: the role of nanotube surface area. Nano Lett. 4, 353–356. https://doi.org/10.1021/nl035009o.

César, N.R., Pereira-da-Silva, M.A., Botaro, V.R., de Menezes, A.J., 2015. Cellulose nanocrystals from natural fiber of the macrophyte Typha domingensis: extraction and characterization. Cellulose 22, 449–460. https://doi.org/10.1007/s10570-014-0533-7.

De Morais Teixeira, E., Corrêa, A.C., Manzoli, A., de Lima Leite, F., de Oliveira, C.R., Mattoso, L.H.C., 2010. Cellulose nanofibers from white and naturally colored cotton fibers. Cellulose 17, 595–606. https://doi.org/10.1007/s10570-010-9403-0.

Dufresne, A., 2017. Nanocellulose: From Nature to High Performance Tailored Materials, Nanocellulose: From Nature to High Performance Tailored Materials. De Gruyter, Berlin. https://doi.org/10.1515/9783110480412.

Eichhorn, S.J., Dufresne, A., Aranguren, M., Marcovich, N.E., Capadona, J.R., Rowan, S. J., Weder, C., Thielemans, W., Roman, M., Renneckar, S., Gindl, W., Veigel, S., Keckes, J., Yano, H., Abe, K., Nogi, M., Nakagaito, A.N., Mangalam, A., Simonsen, J., Benight, A.S., Bismarck, A., Berglund, L.A., Peijs, T., 2010. Review: current international research into cellulose nanofibres and nanocomposites. J. Mater. Sci. 45, 1–33. https://doi.org/10.1007/s10853-009-3874-0.

Freitas, A.C., De Lima, M., Da, P., Ferreira, A.G., Tadei, W.P., Pinto, A.C., Da, S., 2009. Constituintes químicos do caule de Spathelia excelsa (rutaceae) e atividade frente a Aedes aegypti. Química Nova 32, 2068–2072. https://doi.org/10.1590/S0100-40422009000800016.

French, A.D., Santiago Cintrón, M., 2013. Cellulose polymorphy, crystallite size, and the segal crystallinity index. Cellulose 20, 583–588. https://doi.org/10.1007/s10570-012-9833-y.

Gan, P.G., Sam, S.T., Abdullah, M.F. bin, Omar, M.F., 2020. Thermal properties of nanocellulose-reinforced composites: a review. J. Appl. Polym. Sci. 137. https://doi.org/10.1002/app.48544.

Garcia Filho, F., Da, C., Luz, F.S.D.A., Oliveira, M.S., Pereira, A.C., Costa, U.O., Monteiro, S.N., 2020. Thermal behavior of graphene oxide-coated piassava fiber and their epoxy composites. J. Mater. Res. Technol. 9, 5343–5351. https://doi.org/10.1016/j.jmrt.2020.03.060.

García-Guzmán, L., Arzate-Vázquez, I., Velazquez, G., Díaz-Bandera, D., García-Eleno, M. A., Castaño, J., Guadarrama-Lezama, A.Y., 2024. Isolation and characterization of starch, cellulose, and their nanostructures obtained from commelina coelestis willd root. J. Polym. Environ. https://doi.org/10.1007/s10924-024-03210-y.

Ghasemi, S., Espahbodi, A., Gharib, N., Zare, Y., Rhee, K.Y., 2023. Prediction of interphase parameters for nanocellulose composites using a modified Halpin–Tsai approach. Cellulose 30, 9439–9452. https://doi.org/10.1007/s10570-023-05445-9.

Imiete, I.E., Giannini, L., Tadiello, L., Orlandi, M., Zoia, L., 2023. The effect of sulfate half-ester groups on the mechanical performance of cellulose nanocrystal-natural rubber composites. Cellulose 30, 8929–8940. https://doi.org/10.1007/s10570-023-05432-0.

Kalia, S., Dufresne, A., Cherian, B.M., Kaith, B.S., Avérous, L., Njuguna, J., Nassiopoulos, E., 2011. Cellulose-based bio- and nanocomposites: a review. Int. J. Polym. Sci. 2011, 1–35. https://doi.org/10.1155/2011/837875.

Lee, B.-M., Jeun, J.-P., Kang, P.-H., Choi, J.-H., Hong, S.-K., 2017. Isolation and characterization of nanocrystalline cellulose from different precursor materials. Fibers Polym. 18, 272–277. https://doi.org/10.1007/s12221-017-6548-6.

Lin, N., Dufresne, A., 2014. Surface chemistry, morphological analysis and properties of cellulose nanocrystals with gradiented sulfation degrees. Nanoscale 6, 5384–5393. https://doi.org/10.1039/C3NR06761K.

Liu, Y., Hu, H., 2008. X-ray diffraction study of bamboo fibers treated with NaOH. Fibers Polym. 9, 735–739. https://doi.org/10.1007/s12221-008-0115-0.

Martins, D.F., De Souza, A.B., Henrique, M.A., Silvério, H.A., Flauzino Neto, W.P., Pasquini, D., 2015. The influence of the cellulose hydrolysis process on the structure of cellulose nanocrystals extracted from capim mombaça (Panicum maximum. Ind. Crops Prod. 65, 496–505. https://doi.org/10.1016/j.indcrop.2014.10.035.

Martins, C.C.N., Dias, M.C., Mendonça, M.C., Durães, A.F.S., Silva, L.E., Félix, J.R., Damásio, R.A.P., Tonoli, G.H.D., 2021. Optimizing cellulose microfibrillation with NaOH pretreatments for unbleached Eucalyptus pulp. Cellulose 28, 11519–11531. https://doi.org/10.1007/s10570-021-04221-x.

Mathias, S.L., De Assumpção Pereira-da-Silva, M., de Almeida Lucas, A., de Menezes, A. J., 2022. Potential application of cellulose nanocrystals obtained from cultivated fibers in Amazon forest. Ind. Crops Prod. 187, 115426. https://doi.org/10.1016/j.indcrop.2022.115426.

Moreira, W.A.D.S., Lima, M.D.A.P., Ferreira, A.G., Ferreirac, I.C.P., Nakamurac, C.V., 2009. Chemical constituents from the roots of spathelia excelsa and their antiprotozoal activity. J. Braz. Chem. Soc. 20, 1089–1094.

Nam, S., French, A.D., Condon, B.D., Concha, M., 2016. Segal crystallinity index revisited by the simulation of X-ray diffraction patterns of cotton cellulose Iβ and cellulose II. Carbohydr. Polym. 135, 1–9. https://doi.org/10.1016/j.carbpol.2015.08.035.

Nobre, A.D., 2012. Projeto Fênix Amazônico desenvolve novos materiais compósitos com fibras de árvores pioneiras da Amazônia [WWW Document]. Blog. URL ⟨http://fenixamazonico.blogspot.com/2012/05/projeto-fenix-amazonico-desenvolve.html⟩ (accessed 12.6.20).

Paksung, N., Pfersich, J., Arauzo, P.J., Jung, D., Kruse, A., 2020. Structural effects of cellulose on hydrolysis and carbonization behavior during hydrothermal treatment. ACS Omega 5, 12210–12223. https://doi.org/10.1021/acsomega.0c00737.

Pettersen, R.C., 1984. The Chemical Composition of Wood, 57–126. http://doi.org/10.1021/ba-1984-0207.ch002.

Rao, H.J., Senthamaraikannan, P., Suyambulingam, I., Parameswaranpillai, J., Priyadharshini, G.S., Senthilkumar, B., 2024. Isolation and characterization of novel natural fiber from Streblus asper. Biomass Convers. Biorefin. https://doi.org/10.1007/s13399-024-06136-6.

Revol, J.F., Dietrich, A., Goring, D.A.I., 1987. Effect of mercerization on the crystallite size and crystallinity index in cellulose from different sources. Can. J. Chem. 65, 1724–1725. https://doi.org/10.1139/v87-288.

Rodrigues, W.A., 1962. Árvore hapaxanta na flora amazônica. Botânica 14.

Roman, M., Winter, W.T., 2004. Effect of sulfate groups from sulfuric acid hydrolysis on the thermal degradation behavior of bacterial cellulose. Biomacromolecules 5, 1671–1677. https://doi.org/10.1021/bm034519+.

Sánchez-García, M.D., Hilliou, L., Lagarón, J.M., 2010. Morphology and water barrier properties of nanobiocomposites of κ/ι-Hybrid carrageenan and cellulose nanowhiskers. J. Agric. Food Chem. 58, 12847–12857. https://doi.org/10.1021/jf102764e.

Sanjeevi, R., Jafrey Daniel James, D., Senthamaraikannan, P., 2024. Exploration of Cymbopogon nardus root fibers characteristics for sustainable lightweight composite reinforcement applications. Cellulose. https://doi.org/10.1007/s10570-024-06160-9.

Segal, L., Creely, J.J., Martin, A.E., Conrad, C.M., 1959. An empirical method for estimating the degree of crystallinity of native cellulose using the X-ray diffractometer. Text. Res. J. 29, 786–794. https://doi.org/10.1177/004051755902901003.

Sun, X.-F., Fowler, P., Rajaratnam, M., Zhang, G., 2010. Extraction and characterisation of hemicelluloses from maize stem. Phytochem. Anal. 21, 406–415. https://doi.org/10.1002/pca.1211.

Xie, S., Zhang, X., Walcott, M.P., Lin, H., 2018. Applications of cellulose nanocrystals: a review. Eng. Sci. https://doi.org/10.30919/es.1803302.

Yang, H., Yan, R., Chen, H., Lee, D.H., Zheng, C., 2007. Characteristics of hemicellulose, cellulose and lignin pyrolysis. Fuel 86, 1781–1788. https://doi.org/10.1016/j.fuel.2006.12.013.